Materials & Design 213 (2022) 110343

Contents lists available at ScienceDirect

Materials & Design

journal homepage: www.elsevier.com/locate/matdes

Graph-theoretic estimation of reconfigurability in origami-based metamaterials

Koshiro Yamaguchi [a], Hiromi Yasuda [a,b], Kosei Tsujikawa [c], Takahiro Kunimine [d], Jinkyu Yang [a,*]

[a] William E. Boeing Department of Aeronautics and Astronautics, University of Washington, Seattle, WA 98195-2400, USA
[b] Department of Mechanical Engineering and Applied Mechanics, University of Pennsylvania, Philadelphia, PA 19104, USA
[c] Division of Mechanical Science and Engineering, Graduate School of Natural Science and Technology, Kanazawa University, Kanazawa, Ishikawa 920-1192, Japan
[d] Faculty of Mechanical Engineering, Institute of Science and Engineering, Kanazawa University, Kanazawa, Ishikawa 920-1192, Japan

HIGHLIGHTS

- A graph-based method is proposed to assess reconfigurability in origami metamaterial.
- Tachi-Miura Polyhedron tessellations have an abundance of reconfigurability.
- The heterogeneity and connectivity of unit cells contribute to reconfigurability.
- This method contributes to designing origam metamaterial with tailored properties.

GRAPHICAL ABSTRACT

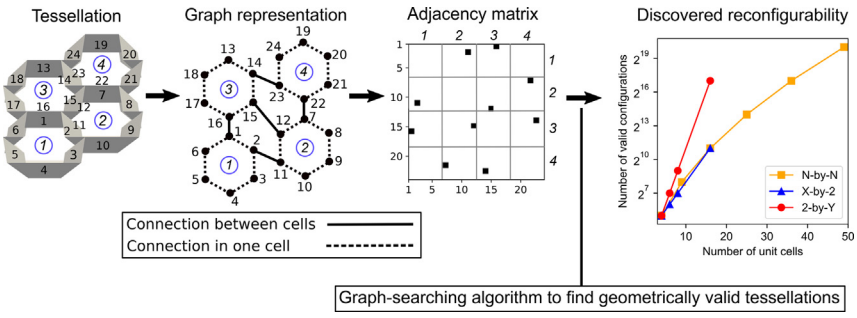

ARTICLE INFO

Article history:
Received 11 July 2021
Revised 9 November 2021
Accepted 20 December 2021
Available online 21 December 2021

Keywords:
Mechanical metamaterials
Graph theory
Reconfigurable systems

ABSTRACT

Origami-based mechanical metamaterials have recently received significant scientific interest due to their versatile and reconfigurable architectures. However, it is often challenging to account for all possible geometrical configurations of the origami assembly when each origami cell can take multiple phases. Here, we investigate the reconfigurability of a tessellation of origami-based cellular structures composed of bellows-like unit cells, specifically Tachi-Miura Polyhedron (TMP). One of the unique features of the TMP is that a single cell can take four different phases in a rigid foldable manner. Therefore, the TMP tessellation can achieve various shapes out of one original assembly. To assess the geometrical validity of the astronomical number of origami phase combinations, we build a graph-theoretic framework to describe the connectivity of unit cells and to analyze the reconfigurability of the tessellations. Our approach can pave the way to develop a systematic computational tool to design origami-based mechanical metamaterials with tailored properties.

1. Introduction

Mechanical metamaterials can have a wide range of mechanical properties by leveraging the design freedom in their architectures [1–3]. Origami has helped this emerging platform to add the tunability of its shapes and behaviors after fabrications [4,5]. Recently, an extensive amount of research on origami-based metamaterials has been conducted to show their various characteristics in both mathematical and mechanical aspects [6–9]. Particular interest has been placed on the realization of reconfigurable mechanical metamaterials via the concept of origami, kirigami, or equivalent architectures [10–17]. While most research focuses on the homogeneous arrangements of origami units and their intrinsic properties, the cross-linkage of heterogeneous origami cells and their effective global characteristics have been relatively unexplored.

* Corresponding author.
E-mail address: jkyang@aa.washington.edu (J. Yang).

https://doi.org/10.1016/j.matdes.2021.110343
0264-1275/

To address this connectivity and reconfigurability problem of heterogeneous origami architectures, Tachi-Miura Polyhedron (TMP) can serve as an ideal platform [18,14]. TMP is one of the origami-based mechanical metamaterials with bellows-like 3D unit cells composed of two different sheets (Fig. 1a). This TMP-based metamaterial features several mechanical characteristics, such as flat and rigid foldability, negative Poisson's ratio, multistability, and load-bearing capabilities [19,14]. Notably, each TMP cell can take four different states (i.e., phases) while maintaining rigid foldability. Specifically, in addition to the well-known bellows-like TMP state, by flattening certain creases of the structure, we can achieve origami tube minus (OT−, which is a left-parallelepiped tube) and origami tube plus (OT+, a right-parallelepiped tube) (Fig. 1b). Furthermore, by flattening all creases, we can obtain a defect state that does not hold any volume (See Fig. 1c for all four states). Thus, when we combine them into a multi-cell structure, we can construct a tessellation of heterogeneous origami cells. However, we cannot arbitrarily assign one of four states to each unit cell randomly, because it can result in a geometrically invalid configuration. Therefore, we have to consider connectivity of TMP cells and find a method to discover geometrically valid tessellations efficiently. If we follow the brute-force method, the number of possible configurations that need to be assessed becomes 4^n, where n is the total number of the TMP cells. This exponential increase of the search space is often called the "curse of dimensionality", also known as the combinatorial explosion. This leads the search for the geometrically valid configuration impossible for a large tessellation.

To overcome this hurdle, we can consult the graph-theoretic method to describe and analyze the TMP-based tessellations. Graph theory is a field in discrete mathematics, which is used to represent pairwise relations between objects [20]. In this mathematical schematization, the objects are referred to as vertices, and the connected pairs of the objects are called edges. In diagrammatic ways, graphs are often represented with dots (or circles) for vertices and lines for edges. Generally, graphs are classified into

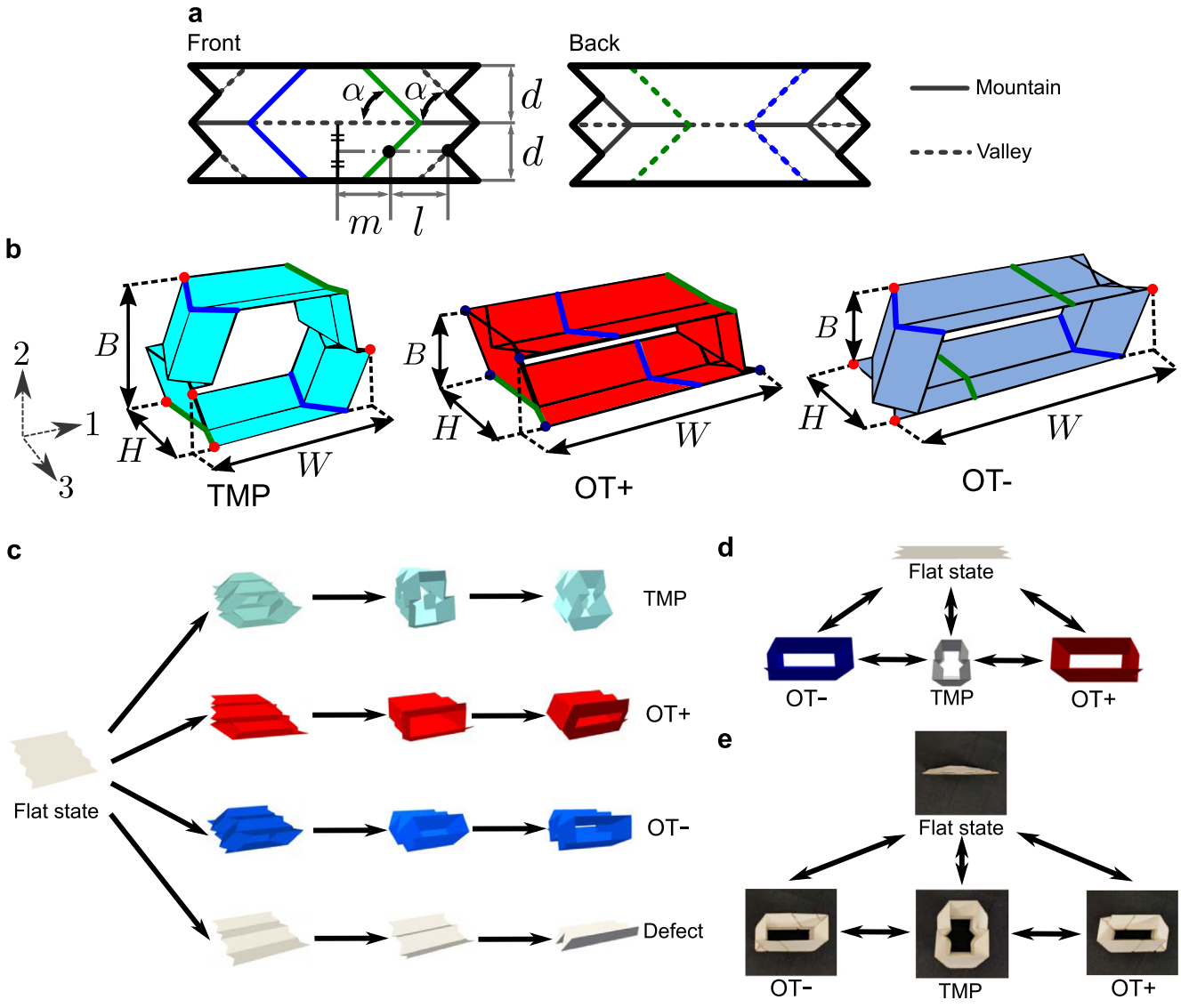

Fig. 1. Folding behavior of a single Tachi-Miura Polyhedron (TMP) unit cell. **a**, crease patterns and geometrical parameters of two flat sheets composing the TMP. **b**, the folding angles of blue and green creases decide the reconfigurable states of a unit cell. When blue (green) creases are folded flat, the unit cell takes the OT+ (OT−) phase. Dimensions B, W, and H correspond to the width, breadth, and height of the structure, respectively. Also, axis numbers 1, 2, and 3 have the same direction as width, breadth, and height, respectively. **c**, 3D rendered images of the transition from the flat state to four reconfigurable states. **d**, 3D rendered images of a TMP unit cell with the initial flat state and the three reconfigurable states of TMP, OT+, and OT−. **e**, images of paper prototypes with corresponding configurations to **d**. (For interpretation of the references to colour in this figure legend, the reader is referred to the web version of this article.)

two types: undirected graphs and directed graphs. The former have edges without direction (two-way relationship), whereas the latter has edges with direction (one-way relationship). This simple-yet-efficient mathematical structure can be utilized to model various types of connections in general. Therefore, it has been applied to numerous systems, such as physical [21], biological [22], and information [23] ones. However, this versatile feature of graph theory has not been fully leveraged to model and analyze tessellations of mechanical metamaterials composed of unit cells, to the best of the authors' knowledge.

In this work we aim at: (i) estimating the total number of valid configurations of TMP tessellations; and (ii) assessing the reconfigurability and the resultant tunability of the mechanical properties in the TMP tessellations. By using the efficient graph-theoretic algorithm we develop, we achieve high efficiency in calculating all possible combinations of TMP cells in a given tessellation. We find that the computation time by this graph-theoretic approach is 20 to 100 times faster than the brute-force (slowest) algorithm as a benchmark. As an outcome of this calculation, we find that TMP tessellation has the vast possibility to manipulate both mechanical properties and shape in an efficient and controllable manner. Thanks to the versatile nature of TMPs, this mechanical platform can achieve various unique characteristics simultaneously: rich heterogeneity, flat-foldability, negative Poisson's ratio, reconfigurability after fabrication, 3D-space filling feature, and tunability in terms of mechanical properties and shape. Thus, such versatility is the advantage of the proposed system over those investigated in the previous research works [24,13,17,12,10,25,26]. While this platform can be applied to various mechanical, aerospace, and medical purposes, we specifically note that two engineering applications: one is the structures for space engineering where the flat-foldability and reconfigurability after fabrication are important due to the rigorous volumetric requirement in the rocket fairings and scarce launch opportunities. Another application is human bones where the combination of positive and negative Poissonś ratio and wide range of mechanical tunability are required [27]. The graph-theoretic approach developed herein will be useful in a broad spectrum of scientific and engineering disciplines.

2. Methods and materials

2.1. TMP tessellation and its transformation

It is well known that TMP can take finite volume or be collapsed to zero volume during its folding process [19] (see "TMP" and "flat" state in Fig. 1). In this study, we also consider two other geometries, so-called origami tube minus and origami tube plus, which can be generated from the flat state without deviating from the rigid-foldable assumption (see Supplementary Movie 1 for the demonstration of a paper prototype, and Supplementary Movie 2 for the 3D rendered transformation). Thus, in this study, we consider four possible states of unit cells: TMP, OT−, OT+, and Defect. Here, defect mode means the flat state, which does not occupy any volume.

Fig. 1(a) explains the components of TMPs with geometrical parameters (l, m, d, α). In Fig. 1(b), we see that the folding angle of blue and green creases decides the reconfigurable states of a unit cell. If blue (green) creases are folded flat, unit cells become OT+ (OT−). Fig. 1(c) shows the transition of the unit cell from the flat state to four reconfigurable states of TMP, OT+, OT−, and Defect. Fig. 1(d) and (e) depict those states and transformations between them for the 3D-rendered model and paper prototype, respectively.

The TMP cells can further be assembled into a tessellation in both horizontal and vertical manner as shown in Fig. 2(a), and it can have multiple cells with different states (see Supplementary Movie 3 for a transformation of the tessellation). For example, Figs. 2(b) and (c) show some exemplary configurations of the 3-by-3 tessellation in the 3D-rendered graphics and the corresponding paper prototype images. Here, TMP, OT−, and OT+ are represented by gray, blue, and red colors, respectively. By including the defect mode, we have four different states that can be assigned for each unit. Therefore, we can consider 4^n patterns of configurations within a n-cell tessellation. However, there exists a kinematic relationship between the adjoined TMP cells, and a large portion of the 4^n patterns are not valid. Fig. 3 illustrates this problem by using two-cell and three-cell tessellations. By simulating the stacking of unit cells, we can tell that some configurations are invalid due to the unmatching of the geometrical boundaries of the unit cells.

While we can achieve various shapes with this reconfigurable origami tessellation, it is hard to know the actual number of total configurations within a given size of tessellation. Considering all cases (e.g., 4^9 = 262,144 for 3-by-3 TMP tessellations) and sorting out what are valid configurations one by one is computationally expensive and even impossible for a large tessellation using conventional computational power. To overcome this hurdle, we introduce the idea of a graph-theoretic framework to discover the possible configuration efficiently. With the aid of the graph representation of a reconfigurable origami tessellation and adjacency matrix obtained from the graph information, we are able to calculate the total number of valid configurations systematically. In the following sections, we introduce the graph representation and adjacency matrices to assess the combinatorial problem of the TMPs.

2.2. Graph representation of TMP tessellation

Recently, several researchers have tackled tessellation-related problems for materials sciences with the aid of graph-theoretic techniques. Arkus et al. utilized graph-theoretic enumerations of adjacency matrices and distance matrices to find the finite sphere packings [28]. Vlassis et al. applied graphs and graph convolutional deep neural network for anisotropic hyperelasticity of polycrystal materials [29]. Herein, we further leverage this technology to investigate the reconfigurability of origami tessellations.

As a first step, we attempt to translate physical TMP tessellations to graph representations. This idea of extracting characteristic points from the geometry of an origami structure has been previously reported [30]. This simplification of origami-based metamaterials into the lattices of characteristic points shows a great advantage to understand and analyze origami-based metamaterials. Here, we utilize a similar process to schematize TMP tessellations as graph structures. Figs. 4(a) and (b) show how we define an undirected graph $G = (V, E)$ from a single unit cell and a tessellation, respectively. Here, vertices V represent the six major faces of a unit cell, and the edge set E consists of unordered pairs of vertices. The number of vertices is $|V| = 6n$, where n is the number of unit cells in a tessellation. The edge set counts the connections of faces both within one unit cell and between neighboring cells (see dashed and solid lines in Fig. 4). Then, we also define a subgraph $G\prime = (V', E')$ such that $V' \subseteq V$ and $E' \subseteq E$, where V' and E' represents the interconnections among the unit cells. For example, in Fig. 4(b) where we consider a 2-by-2 tessellation, we have $V' = \{1, 2, 7, 11, 12, 14, 15, 16, 22, 23\}$ and $E' = \{(1, 16), (2, 11), (7, 22), (12, 15), (14, 23)\}$.

Based on this graph representation, we utilize graph-theoretic enumeration of adjacency matrices. We introduce those definitions in the following. A tessellation of n unit cells can be described by an

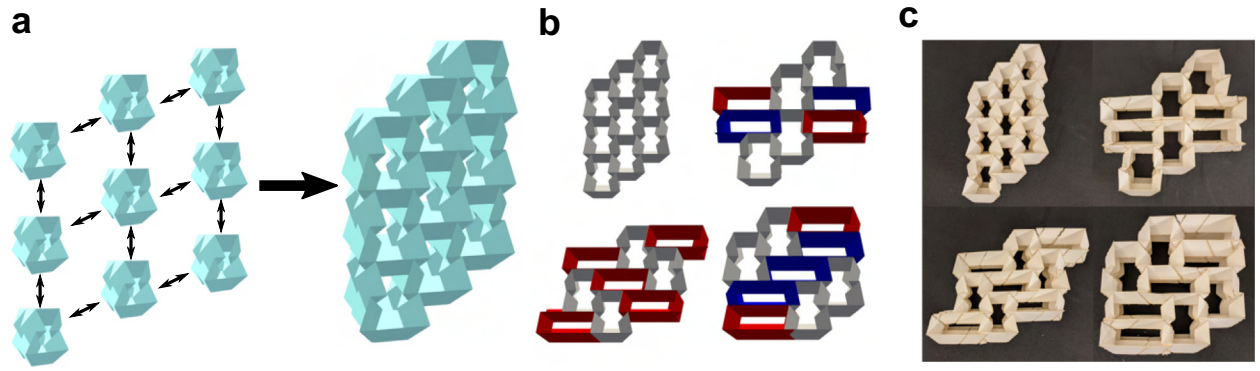

Fig. 2. Connectivity of a 3-by-3 TMP tessellation and examples of its various configurations. **a**, 3D rendered images showing how a tessellation is built with the nine unit cells. Certain faces of unit cells are adjoined altogether to form one tessellation. **b**, 3D rendered images of the 3-by-3 tessellation with four different configurations. **c**, digital images of the paper prototypes corresponding to the four tessellations shown in **b**.

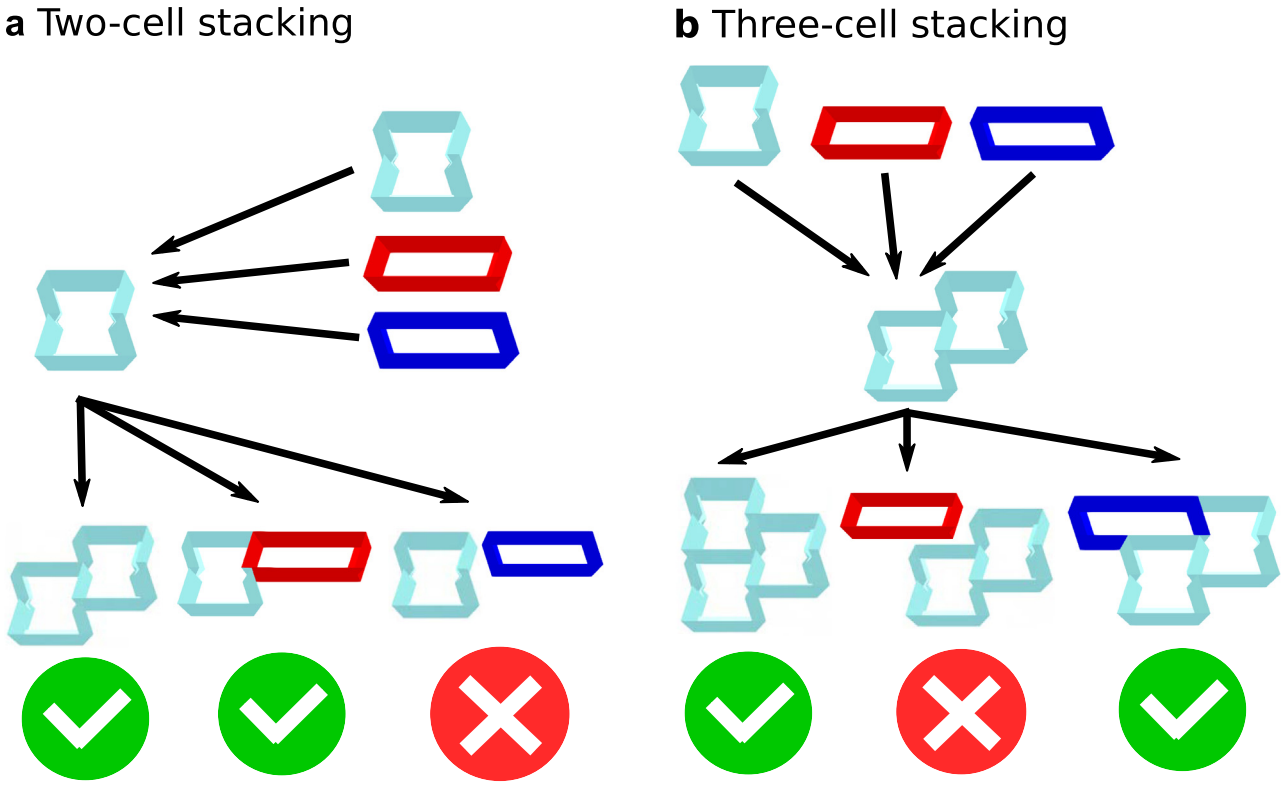

Fig. 3. Geometrical validity check of the TMP tessellation. Cases of **a**, two-cell tessellations and **b**, three-cell tessellations. In **a**, one unit cell (TMP, OT+, or OT−) is attached to one TMP cell. The attachment of TMP and OT+ results in a valid configuration. However, we can see that the OT− tube does not fit with the upper-right side of the TMP cell. Likewise, cases of three-cell stacking in **b** show that the attachment of TMP and OT− to a two-TMP stacking brings the valid configuration, whereas the attachment of OT+ tube makes the tessellation invalid.

$|V| \times |V|$ adjacency matrix $\boldsymbol{A}$. This matrix is defined with the graph G and the subgraph $G\prime$. Therefore it details which vertices (faces in physical unit cells) are in contact: $\boldsymbol{A}_{ij} = 1$ if and only if $(u_i, u_j) \in E'$ and otherwise $\boldsymbol{A}_{ij} = 0$. This means that $\boldsymbol{A}_{ij} = 1$ if ith and jth faces are attached to each other, and $\boldsymbol{A}_{ij} = 0$ if they are not. It should be noted that each x-by-y tessellation has only one unique adjacency matrix – regardless of the phases of unit cells – because once we define the size of the tessellation and its arrangement, we also know which physical faces of unit cells to be connected to others. The illustration of the adjacency matrix is also shown in Fig. 4(b). Here, the dots denote the edge set E', which represents the adjoining of TMP faces.

2.3. Combinatorial search for valid configurations

To analyze the reconfigurability of the TMP tessellations, we utilize the aforementioned graph representation and algorithm. The reconfigurability can be quantified by the number of unique configurations that the tessellation can achieve. The search of valid configurations consists of three steps: (i) definition of the size of tessellation, (ii) graph representation and graph-theoretic enumeration of the tessellation, and (iii) combinatorial search for valid configurations. First, we define the size and shape of the tessellation. Our graph-theoretic method is versatile and applicable to various types of tessellations. However, in order to make comparisons

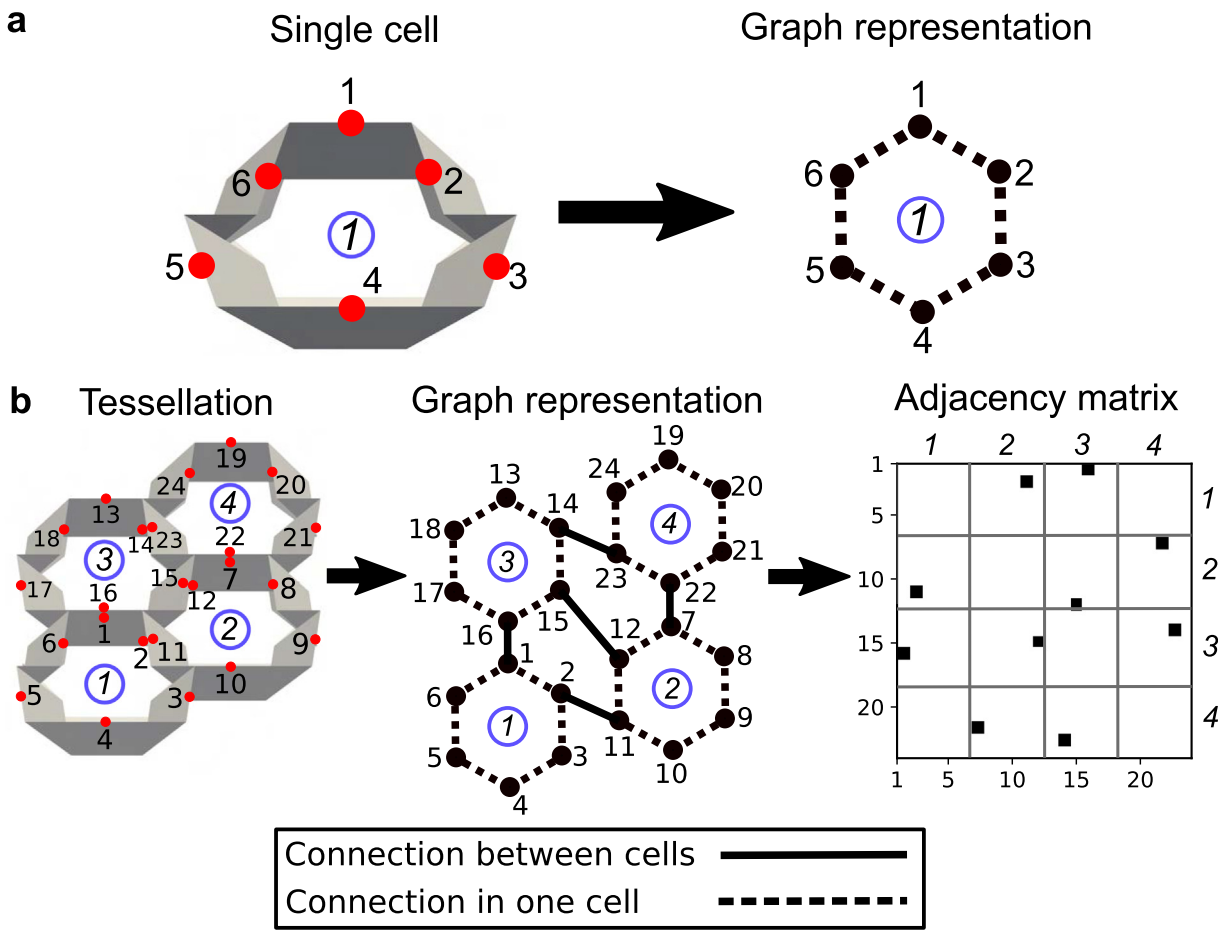

Fig. 4. Examples of the graph representation for **a**, a single unit cell and **b**, a 2-by-2 tessellation. Red dots in **a** and **b** represent the midpoints of the major side edges of TMPs (adjacent red dots in **b** are actually overlapping). In a graph representation, those red dots are considered as nodes. Dashed lines in **a** and **b** mean the connection of the nodes within a unit cell. Solid lines in **b** mean the connection of the nodes between different unit cells. Italic numbers in blue circles denote the TMP unit cells, and upright numbers denote the middle points in physical TMPs and the corresponding nodes in the graph. In the illustration of the adjacency matrix, the left and bottom labels show the node numbers as represented in the graph. Likewise, right and top labels in italic numbers denote the TMP unit cells. Gray lines in the adjacency matrix show which part of the matrix corresponds to the TMP unit cell numbers. Dots in this adjacency matrix indicate the connected nodes, i.e., adjoined faces in the TMP tessellation.

and measure the effectiveness of the unit cell number on the reconfigurability, we use a rectangular arrangement of *X*-by-*Y* tessellation, where *X* and *Y* are the number of unit cells in horizontal and vertical directions, respectively.

Secondly, we represent the tessellation via a graph and enumerate the information about the connection of the unit cells using an adjacency matrix. Again, the adjacency matrix is unique for each tessellation and immutable in the process of tessellation search. After establishing the information about tessellations, we move to the final step, which is the combinatorial search for valid configurations. In this step, we utilize the complete list of 3-cell configurations that are known a priori. It has 32 configurations as shown in Supplementary Figure S2, and we combine those 3-cell configurations to find configurations of larger tessellations.

The schematic illustration of the process of this combinatorial search is shown in Fig. 5. The top row shows the graphical evolution of the TMP tessellation, the middle row shows their graph representation, and the bottom panel explains how we use adjacency matrices for this search process. Italic numbers with red boxes show that unit cells have assignments of configurations, whereas italic numbers with no boxes show that those unit cells do not have assignments yet. By using this assignment information and adjacency matrix, we detect an unassigned unit cell that is adjacent to the assigned ones. Blue arrows and boxes in the matrix show the process of searching for an adjacent unit cell to assign. To begin the search, we allocate configurations to the three cells at the lower-left end. Then, based on the graph structure, we find an adjacent cell and assign a configuration to the adjacent one by looking up the list of the 3-cell configurations (see gray triangles in Fig. 5b). We repeat this process until all unit cells have configurations. Also, in this process, we check every one of the configurations in the list. Therefore, at the end of the process, we can count all valid configurations out of a given size of tessellation.

3. Results and discussion

3.1. Estimation and growth of reconfigurability

We start discussing the number and growth of reconfigurability by changing the size of tessellations. The result of the searching for the number of valid configurations with 14 different tessellation sizes is summarized in Figs. 6(a) and (b) for selected results and Table 1 for all results. To verify the result from our graph-theoretic method, we also implement a brute-force method for smaller sizes of tessellations as explained in Supplementary Note A. We start to examine the unique configurations with 2-by-2 tessellations with the total number of four unit cells. We then enlarge the size of the tessellation by adding a row or a column of unit cells up to 49 unit cells in total. If we follow the brute-force method for

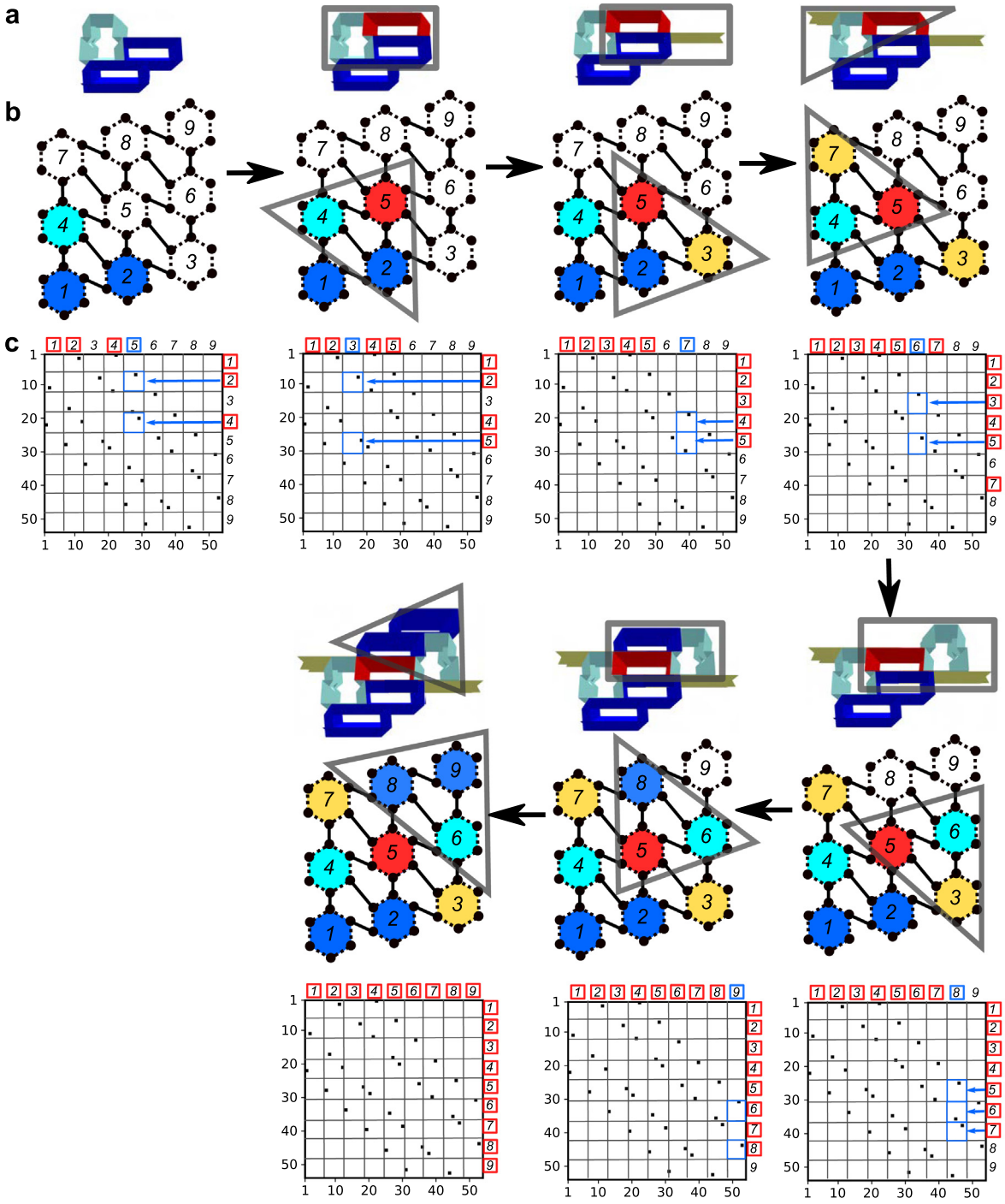

Fig. 5. An example of discovering a valid configuration for the 3-by-3 tessellation with logistic illustrations of the computation processes using adjacency matrices. In **a** and **b**, cyan, red, blue, and yellow colors in the graph representation correspond to the TMP, OT+, OT−, and defect states of the unit cell, respectively. In **a**, 3d-rendered images represent the graphical process of building tessellations. Likewise, in **b**, the pictures of graphs with colored parts show the schematic process of the tessellation search. Three unit cells enclosed by gray lines in **a** and **b** indicate where the 3-cell configurations are referenced and adopted. In **c**, adjacency matrices are illustrated in the same way as Fig. 4(b). Italic numbers with red boxes show that unit cells have assignments of configurations, whereas italic numbers with no boxes show that those unit cells do not have assignments yet. Blue arrows and boxes in the matrix show the process of searching an adjacent unit cell to assign the proper unit cell configuration.

this number of unit cells, we have to investigate $4^{49} \approx 10^{29}$ candidates of configurations that are almost impossible to examine even with the aid of high-performance computers. Fig. 6(c) shows the comparison of computation time between brute-force and graph-based methods. In terms of computation time, our graph-based method is generally 20 to 100 times faster than the brute-force method to search configurations from 2-by-2 to 5-by-5 tessellations with a personal desktop computer. Therefore, by utilizing our method, we achieve a substantial amount of efficiency in estimating the reconfigurability of the origami-based metamaterials.

As we increase the size of the tessellation, we see that the number of unique configurations increases exponentially for X-by-2 and 2-by-Y cases where X and Y are the number of horizontal and vertical stacking, respectively. For N-by-N tessellation where

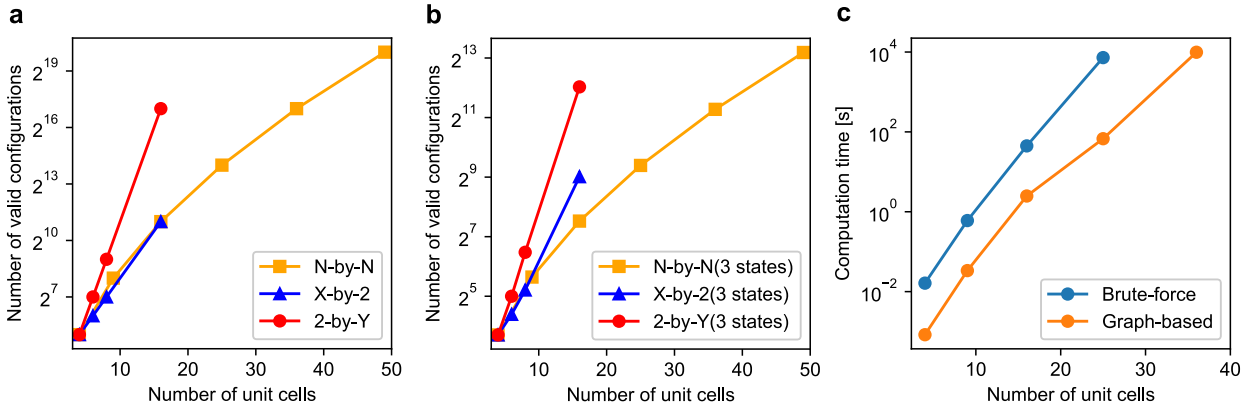

Fig. 6. The number of valid configurations and computation time for each tessellation size. **a**, 14 results of counting valid configurations with four configurations (TMP, OT+, OT−, and Defect) based on the categorization of N-by-N, X-by-2, and 2-by-Y tessellations where X, Y, and N are the number of horizontal and vertical stackings of the tessellation. **b**, 14 results of counting valid configurations with three configurations (OT+/OT−/Defect, TMP/OT+/Defect, TMP/OT−/Defect, and TMP/OT+/OT−). Each three-state configuration has the same number of valid configurations. Other results and exact numbers are shown in Table 1. **c**, a comparison of computation time between brute-force and graph-based methods. The results of 2-by-2, 3-by-3, 4-by-4, and 5-by-5 tessellations are used for the brute-force method. Besides those tessellations, an additional result of 6-by-6 tessellations is shown for the graph-based method.

Table 1
Number of unique configurations for various tessellation sizes.

Size	4 states	3 states	Increase	Size	4 states	3 states	Increase
2-by-2	32	13	146%	3-by-4	1024	120	753%
3-by-2	64	21	205%	4-by-4	2048	184	1013%
2-by-3	128	32	300%	8-by-2	2048	517	296%
4-by-2	128	37	246%	2-by-8	131072	4181	3035%
2-by-4	512	89	475%	5-by-5	16383	672	2338%
3-by-3	256	50	412%	6-by-6	131072	2480	5185%
4-by-3	512	82	524%	7-by-7	1048576	9312	11160%

N is for both horizontal and vertical numbers, we see that the rate of increase decays gradually. Furthermore, we observe that the rate of increase in the number differs by the direction of adding a new column or row (horizontally or vertically). Adding a column of unit cells to the tessellation doubles the unique configurations to the original one, whereas adding a row quadruples them. In Fig. 7, we show an example of adding a row or a column to the 2-by-2 tessellation. While we obtain two different configurations in Fig. 7(b) for 3-by-2 tessellations, we can achieve four configurations for 2-by-3 tessellations in Fig. 7(c). We observe this difference is caused by the direction of the phase transition of unit cells. Since the transition among TMP, OT+, and OT− is lateral movement, the column-wise attachment of unit cells is more bound to the existing tessellations than the row-wise attachment. Actually, a column-wise attachment involves only TMP and OT+ in Fig. 7(b). However, a row-wise addition includes TMP, OT+, OT−, and defects in Fig. 7(c).

Returning to Fig. 6(a), the red line connects the results from 2-by-2, 2-by-3, 2-by-4, and 2-by-8 tessellations. Likewise, the blue line connects the results from 2-by-2, 3-by-2, 4-by-2, and 8-by-2 tessellations. Both lines show linear growth in $\log_2$ scale along the y-axis because there is a pattern for the growth of the unique configurations, as we state previously. The yellow line shows the results up to 7-by-7 tessellations. Since these results are from the combinations of the horizontal and vertical increments, the increase rate is not constant.

Table 1 also includes the number of unique configurations only with three states (OT+/OT−/Defect, TMP/OT+/Defect, TMP/OT−/Defect, and TMP/OT+/OT−) and the rate of increase of the number of configurations from using three states to four states. Here, each combination of three states (OT+/OT−/Defect, TMP/OT+/Defect, TMP/OT−/Defect, and TMP/OT+/OT−) has the same number of valid configurations and is summarized in Fig. 6(b). The comparison with the four states indicates that each TMP state equally contributes to the excessive growth of reconfigurability. However, one of the advantages of inducing defect states is that we can achieve an enormous variety of reconfigurable shapes without incurring volume increases. Based on the graph-theoretic evaluations, we confirm that the increase of the phase number from three to four contributes directly to the surge of the overall variety of the tessellations. Further results and discussions about the effect of defect modes are included in Supplementary Note B.

3.2. Highly heterogeneous configurations

Now we discuss some examples of configurations we discover in the search process. Figs. 8(a)-(d) show the four examples of anomalous configurations in 4-by-4 tessellations. Each configuration consists of four different states (TMP, OT+, OT−, and Defect), and the composition of the states is highly mixed and distributed within the tessellation. For example, a tessellation in Fig. 8(a) consists of six TMPs, two OT+, six OT−, and two Defects. We again note in passing that unlike normal configurations that have a homogeneous occurrence of deformation states, such heterogeneous configurations composed of a variety of the different states are hard to be discovered by human heuristics.

In addition to the heterogeneity of the configurations, we find that they have tunability in terms of Poisson's ratio and mechanical properties. Here, we examine two Poissonś ratios ν_{HB} and ν_{HW} defined as follows:

$$\nu_{HB} = -\frac{dB/B}{dH/H}, \quad \nu_{HW} = -\frac{dW/W}{dH/H}. \tag{1}$$

Revisit Fig. 1(b) for the definitions of H and B. Fig. 8(e) shows the change of Poisson's ratio ν_{HB} from the folding angle of 0° to 90°.

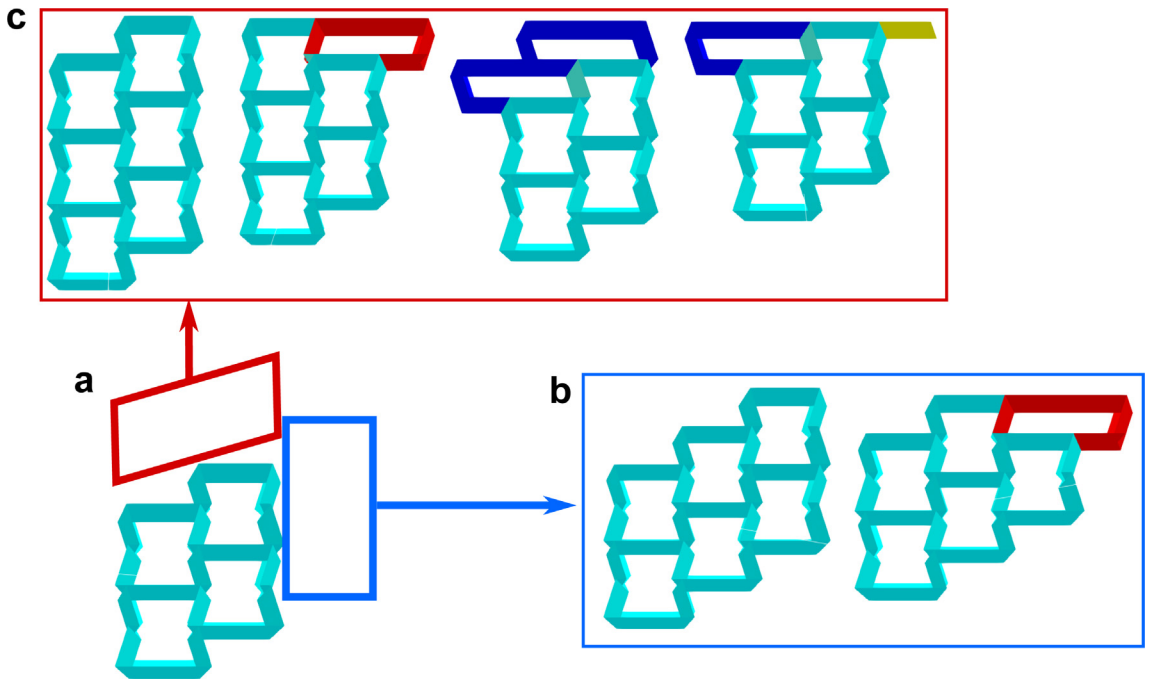

Fig. 7. **a**, an image of a 2-by-2 tessellation with four TMPs. Red box shows the position where the unit cells are attached to build 2-by-3 tessellations. Likewise, blue box shows the position for 3-by-2 tessellations. **b**, 3-by-2 valid tessellations that are emerged from a 2-by-2 tessellation with four TMPs shown in **a**. **c**, 2-by-3 valid tessellations that are emerged from a 2-by-2 tessellation with four TMPs shown in **a**. In both **b** and **c**, these tessellations are the only ones that can emerge from the 2-by-2 tessellation in **a**. Cyan, red, blue, and yellow colors in the 3D rendered images correspond to the TMP, OT+, OT−, and defect states of the unit cell, respectively.

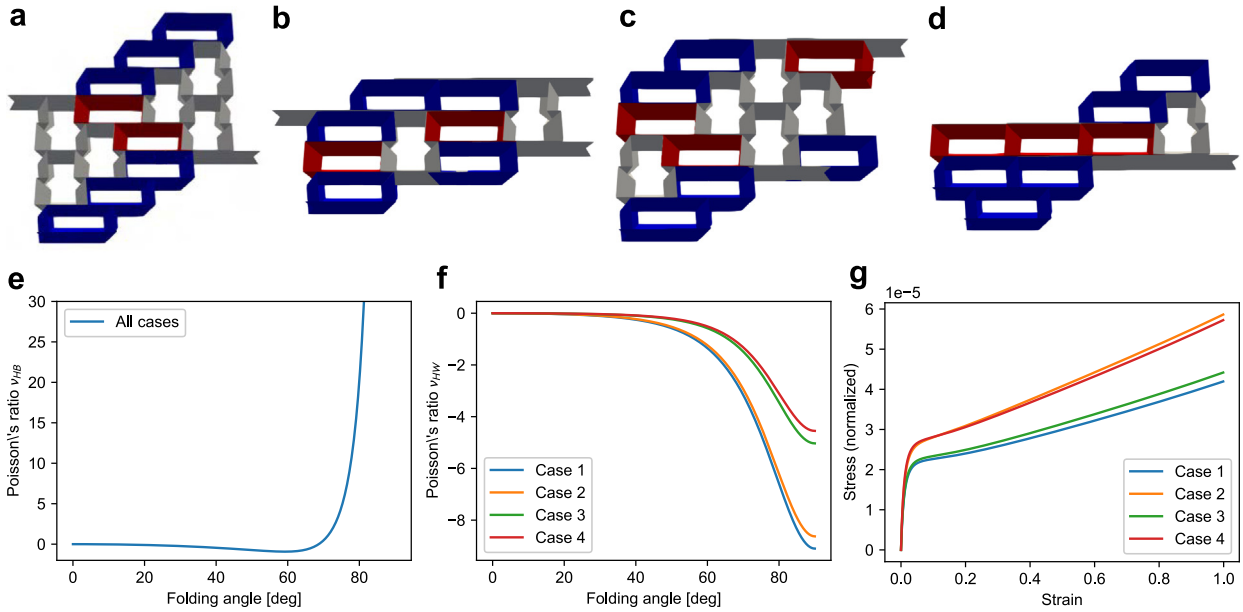

Fig. 8. Examples of heterogeneous configurations in 4-by-4 tessellations and their Poisson's ratio and mechanical responses. **a**, a configuration consisting of 6 TMPs, 2 OT+, 6 OT−, and 2 defects (Case 1). **b**, a configuration consisting of 2 TMPs, 2 OT+, 5 OT−, and 7 defects (Case 2). **c**, a configuration consisting of 5 TMPs, 3 OT+, 5 OT−, and 3 defects (Case 3). **d**, a configuration consisting of 1 TMP, 3 OT+, 5 OT−, and 7 defects (Case 4). **e**, Poisson's ratio between height and breadth directions. For all cases, Poisson's ratio ν_{HB} is identical. **f**, Poisson's ratio ν_{HW} between height and width directions. **g**, Stress–strain relationship of four cases. Here, stresses are calculated with normalized forces.

Throughout the folding stage, ν_{HB} becomes both positive and negative (auxetic). While ν_{HB} is identical for all cases in Fig. 8(e), Poisson's ratio ν_{HW} in Fig. 8(f) is different for each configuration and always negative. These results suggest that we can tune one Poisson's ratio while keeping a property in another direction. Besides, the stress–strain relationships are shown in Fig. 8(g) where we define a cross-sectional area as the area occupied by the tessellations. Here, stress is obtained by using normalized force $F\prime$. Base on this result, we can obtain normalized Youngś modulus of the direction of height (3-axis) $E\prime_3$ at 2% strain for each configuration defined as follows:

$$E\prime_3 = \frac{\sigma\prime_3}{\epsilon_3|_{2\%}} \tag{2}$$

For case 1 to 4 in Fig. 8, the values are $2.13 \times 10^{-3}, 2.55 \times 10^{-3}$, 2.19×10^{-3}, and 2.67×10^{-3}, respectively. We note that those

values are calculated using normalized force, therefore they do not have dimensions and we can apply the material properties once we decide the material to use for the manufacturing. The details of the mechanical analysis are described in Supplementary Note C.

We further extend this result to see if they can simulate specific geometries because such reconfigurability is one of the essential aspects when we utilize these mechanical metamaterials for engineering applications. To assess how much the tessellation's reconfigurability contributes to the ability to simulate the real-life objects, we examine cross-sections of 4-by-4 tessellations and compare them with some images in Supplementary Note D. The result of simulating mechanical properties and the various types of geometries (chair, buffalo, boot, and boat) suggests that this platform of TMP tessellations has a great potential to satisfy the mechanical and geometrical requirements for various engineering applications. Furthermore, this rich versatility of TMP tessellations manifests the importance of efficient methods to find valid configurations because it contributes not only to the fundamental problems of mathematical/geometrical combinations, but also to the design of advanced mechanical metamaterials.

4. Conclusion

In this study, we have demonstrated a graph-theoretic approach to discover the valid configurations of TMP tessellations. Given the challenges of combinatorial problems of origami-based mechanical metamaterials, we have built a computationally efficient framework to account for a complete set of reconfigurable shapes of the TMP tessellations. To this end, we have enumerated the information about the connections of the TMP unit cells using adjacency matrices. One of the unique features of this versatile graph-theoretic approach is that it has the possibility to be applied for designing various types of mechanical metamaterials. This simple approach of using adjacency matrices has proposed an efficient method to describe and analyze the tessellation of the mechanical metamaterials. The result of the aforementioned analysis indicates that the TMP tessellations have an abundance of reconfigurability owing to the heterogeneity of the TMP cells and their versatile connectivity. Besides, the analysis of mechanical properties, such as Poisson's ratio and elastic modulus, suggests that the various configurations of the tessellations yield a wide range of design space. Such reconfigurability can be exponentially improved by adopting a larger number of TMP cells in the tessellation, and the exact number of possible configurations has been calculated by the proposed graph-theoretic method in an accurate and efficient manner.

Given the simplicity of this framework, the graph-based approach can be applied to the other types of the tessellations of mechanical metamaterials (e.g., metal–organic hinged cube tessellation [31], voxelated mechanical metamaterials [10,32], and other origami lattices in 2D or 3D settings [33,15,24,34,16]) by building graph representations for each architecture of mechanical metamaterials and by understanding the connections within the tessellations. For instance, 3D stacked miura-ori variant mechanical metamaterials[16] have multistability in their unit cells that is similar to TMP unit cells. Furthermore, they can form tessellations. Therefore, there is a rich reconfigurability, and the analysis using this graph-based framework can be highly useful. Also, the ability to simulate the various mechanical responses, shapes and morphologies suggest the possibility of answering the following question; given the target geometry and properties we want to achieve, can we dial-in the local phases in unit cells and find the optimal metamaterial configurations globally? This can be assessed by utilizing the graph-theoretic framework developed herein and combining it with combinatorial optimization techniques.

CRediT authorship contribution statement

Koshiro Yamaguchi: Conceptualization, Methodology, Investigation, Software, Visualization, Writing- Original draft preparation. **Hiromi Yasuda:** Conceptualization, Methodology, Investigation, Software, Visualization, Writing - Review & Editing. **Kosei Tsujikawa:** Investigation, Software. **Takahiro Kunimine:** Supervision, Writing - Review & Editing. **Jinkyu Yang:** Conceptualization, Supervision, Writing - Review & Editing, Funding acquisition.

Declaration of Competing Interest

The authors declare that they have no known competing financial interests or personal relationships that could have appeared to influence the work reported in this paper.

Acknowledgments

K.Y. and J.Y. are grateful for the support from the U.S. National Science Foundation (1553202 and 1933729) and the Washington Research Foundation. K.Y. is supported by the Funai Foundation for Information Technology. We thank Dr. Dillon Foight and Prof. Mehran Mesbahi at the University of Washington, and Dr. Jesse Silverberg at Multiscale Systems for helpful discussions.

Appendix A. Supplementary material

Supplementary data associated with this article can be found, in the online version, at https://doi.org/10.1016/j.matdes.2021.110343.

References

[1] S. Babaee, N. Viard, P. Wang, N.X. Fang, K. Bertoldi, Harnessing Deformation to Switch on and off the Propagation of Sound, Adv. Mater. 28 (8) (2016) 1631–1635, https://doi.org/10.1002/adma.201504469.
[2] O.R. Bilal, A. Foehr, C. Daraio, Reprogrammable Phononic Metasurfaces, Adv. Mater. 29 (39), https://doi.org/10.1002/adma.201700628.
[3] Z. Wu, Y. Zheng, K.W. Wang, Metastable modular metastructures for on-demand reconfiguration of band structures and nonreciprocal wave propagation, Phys. Rev. E 97 (2). arXiv:1709.01800, https://doi.org/10.1103/PhysRevE.97.022209.
[4] M. Schenk, S.D. Guest, Geometry of Miura-folded metamaterials, Proceedings of the National Academy of Sciences of the United States of America 110 (9) (2013) 3276–3281, https://doi.org/10.1073/pnas.1217998110.
[5] S. Felton, M. Tolley, E. Demaine, D. Rus, R. Wood, A method for building self-folding machines, Science 345 (6197) (2014) 644–646, https://doi.org/10.1126/science.1252610.
[6] T. Tachi, Introduction to Structural Origami, Journal of the International Association for Shell and Spatial Structures 60 (1) (2019) 7–18, https://doi.org/10.20898/j.iass.2019.199.004.
[7] D. Rus, M.T. Tolley, Design, fabrication and control of origami robots, Nature Reviews Materials 3 (6) (2018) 101–112, https://doi.org/10.1038/s41578-018-0009-8.
[8] L.R. Meza, A.J. Zelhofer, N. Clarke, A.J. Mateos, D.M. Kochmann, J.R. Greer, Resilient 3D hierarchical architected metamaterials, Proceedings of the National Academy of Sciences of the United States of America 112 (37) (2015) 11502–11507, https://doi.org/10.1073/pnas.1509120112.
[9] S. Janbaz, N. Noordzij, D.S. Widyaratih, C.W. Hagen, L.E. Fratila-Apachitei, A.A. Zadpoor, Origami lattices with free-form surface ornaments, Science Advances 3 (11). doi:10.1126/sciadv.aao1595.
[10] N. Yang, C.W. Chen, J. Yang, J.L. Silverberg, Emergent reconfigurable mechanical metamaterial tessellations with an exponentially large number of discrete configurations, Materials and Design 196. doi:10.1016/j.matdes.2020.109143.
[11] J.T. Overvelde, T.A. de Jong, Y. Shevchenko, S.A. Becerra, G.M. Whitesides, J.C. Weaver, C. Hoberman, K. Bertoldi, A three-dimensional actuated origami-inspired transformable metamaterial with multiple degrees of freedom, Nature Communications 7 (1) (2016) 10929, https://doi.org/10.1038/ncomms10929.
[12] J.T.B. Overvelde, J.C. Weaver, C. Hoberman, K. Bertoldi, Rational design of reconfigurable prismatic architected materials, Nature 541 (7637) (2017) 347–352, https://doi.org/10.1038/nature20824.
[13] E.T. Filipov, T. Tachi, G.H. Paulino, D.A. Weitz, Origami tubes assembled into stiff, yet reconfigurable structures and metamaterials, Proceedings of the

National Academy of Sciences of the United States of America 112 (40) (2015) 12321–12326, https://doi.org/10.1073/pnas.1509465112.
[14] H. Yasuda, B. Gopalarethinam, T. Kunimine, T. Tachi, J. Yang, Origami-Based Cellular Structures with In Situ Transition between Collapsible and Load-Bearing Configurations, Adv. Eng. Mater. 21 (12) (2019) 1900562, https://doi.org/10.1002/adem.201900562.
[15] H. Fang, S.-C.A. Chu, Y. Xia, K.-W. Wang, Programmable Self-Locking Origami Mechanical Metamaterials, Adv. Mater. 30 (15) (2018) 1706311, https://doi.org/10.1002/adma.201706311.
[16] Z. Liu, H. Fang, J. Xu, K.W. Wang, A novel origami mechanical metamaterial based on Miura-variant designs: exceptional multistability and shape reconfigurability, Smart Mater. Struct. 30 (8) (2021) 085029, https://doi.org/10.1088/1361-665X/AC0D0F.
[17] B. Haghpanah, L. Salari-Sharif, P. Pourrajab, J. Hopkins, L. Valdevit, Multistable Shape-Reconfigurable Architected Materials, Adv. Mater. 28 (36) (2016) 7915–7920, https://doi.org/10.1002/adma.201601650.
[18] T. Tachi, K. Miura, Rigid-foldable cylinders and cells, Journal of the International Association for Shell and Spatial Structures 53 (174) (2012) 217–226.
[19] H. Yasuda, J. Yang, Reentrant Origami-Based Metamaterials with Negative Poisson's Ratio and Bistability, Phys. Rev. Lett. 114 (18) (2015) 185502, https://doi.org/10.1103/PhysRevLett.114.185502.
[20] M. Mesbahi, M. Egerstedt, Graph Theoretic Methods in Multiagent Networks., Vol. 33 of Princeton Series in Applied Mathematics, Princeton University Press/DeGruyter, 2010.
[21] N. Deo, Graph Theory with Applications to Engineering and Computer Science (Prentice Hall Series in Automatic Computation), Prentice-Hall Inc, USA, 1974.
[22] A.A. Canutescu, A.A. Shelenkov, R.L. Dunbrack, A graph-theory algorithm for rapid protein side-chain prediction, Protein Sci. 12 (9) (2003) 2001–2014, https://doi.org/10.1110/ps.03154503.
[23] K. Xu, W. Hu, J. Leskovec, S. Jegelka, How powerful are graph neural networks?, in: International Conference on Learning Representations, 2019.
[24] J.L. Silverberg, A.A. Evans, L. McLeod, R.C. Hayward, T. Hull, C.D. Santangelo, I. Cohen, Using origami design principles to fold reprogrammable mechanical metamaterials, Science 345 (6197) (2014) 647–650, https://doi.org/10.1126/science.1252876.
[25] M. Ye, L. Gao, H. Li, A design framework for gradually stiffer mechanical metamaterial induced by negative Poisson's ratio property, Materials and Design 192. doi:10.1016/j.matdes.2020.108751.
[26] D. Melancon, B. Gorissen, C.J. García-Mora, C. Hoberman, K. Bertoldi, Multistable inflatable origami structures at the metre scale, Nature 592 (7855) (2021) 545–550, https://doi.org/10.1038/s41586-021-03407-4.
[27] H.M. Kolken, S. Janbaz, S.M. Leeflang, K. Lietaert, H.H. Weinans, A.A. Zadpoor, Rationally designed meta-implants: A combination of auxetic and conventional meta-biomaterials, Materials Horizons 5 (1) (2018) 28–35, https://doi.org/10.1039/c7mh00699c.
[28] N. Arkus, V.N. Manoharan, M.P. Brenner, Deriving finite sphere packings, SIAM Journal on Discrete Mathematics 25 (4) (2011) 1860–1901, https://doi.org/10.1137/100784424. arXiv:1011.5412.
[29] N.N. Vlassis, R. Ma, W.C. Sun, Geometric deep learning for computational mechanics Part I: Anisotropic Hyperelasticity, Comput. Methods Appl. Mech. Eng. 371 (2020) 113299. arXiv:2001.04292.
[30] H. Fang, S. Li, M. Thota, K.W. Wang, Origami lattices and folding-induced lattice transformations, Physical Review Research 1 (2) (2019) 023010, https://doi.org/10.1103/PhysRevResearch.1.023010.
[31] E. Jin, I.S. Lee, D. Kim, H. Lee, W.D. Jang, M.S. Lah, S.K. Min, W. Choe, Metal-organic framework based on hinged cube tessellation as transformable mechanical metamaterial, Science Advances 5 (5). doi:10.1126/sciadv.aav4119.
[32] C. Coulais, E. Teomy, K. De Reus, Y. Shokef, M. Van Hecke, Combinatorial design of textured mechanical metamaterials, Nature 535 (7613) (2016) 529–532. arXiv:1608.00625, doi:10.1038/nature18960.
[33] Y.L. He, P.W. Zhang, Z. You, Z.Q. Li, Z.H. Wang, X.F. Shu, Programming mechanical metamaterials using origami tessellations, Composites Science and Technology 189. doi:10.1016/j.compscitech.2020.108015.
[34] A.A. Evans, J.L. Silverberg, C.D. Santangelo, Lattice mechanics of origami tessellations, Phys. Rev. E 92 (2015) 13205, https://doi.org/10.1103/PhysRevE.92.013205.